Russian Journal of Earth Sciences Online ISSN: 1681-1208

Special Issue: "Kamchatka Earthquake M 8.8 on July 29, 2025"

Coseismic Effect of the 2025 Kamchatka Earthquakes

I. M. Aleshin[1,2], A. A. Soloviev[1,2], A. G. Goev[2], and D. V. Kudin[1]

[1]Geophysical Center, Russian Academy of Sciences, Moscow, Russian Federation
[2]Schmidt Institute of Physics of the Earth, Russian Academy of Sciences, Moscow, Russian Federation
* **Correspondence to:** Igor Aleshin, ima@ifz.ru

Abstract: We investigate the conditions under which coseismic electromagnetic disturbances arise, caused by the propagation of elastic waves from distant earthquakes with magnitudes ranging from 6.9 to 8.7. The origins of these seismic waves were the 2025 Great Kamchatka Earthquake and several strong events in the vicinity of its source. The analyzed data are provided by magnetic observatories of the INTERMAGNET network, which support 1-second recording of the geomagnetic field and are located at distances from 23 to 87 arc degrees from the epicenter of the Great Kamchatka Earthquake. The primary study examines the dependence of the fact of coseismic signal generation on the earthquake magnitude and its epicentral distance. The mechanism underlying coseismic disturbances is not discussed. Effects produced by different seismic phases are considered separately, which determines the lower bound for the epicentral distances under consideration. We show that the electromagnetic signal accompanying the arrival of teleseismic waves is generated only by strong earthquakes with magnitudes $M > 7$. The coseismic effect of the strongest events with magnitudes $M > 7.4$, primarily the Great Kamchatka Earthquake ($M = 8.7$), manifests itself at extremely large epicentral distances, up to 90 arc degrees. We demonstrate that the main spectral component of the coseismic signal occurs in the high-frequency range from 0.05 Hz to 1.0 Hz.

Keywords: Remote earthquakes, magnetic observatory, coseismic electromagnetic effect, 1-second magnetic data, INTERMAGNET, Kamchatka megathrust earthquake

Citation: Aleshin I. M., Soloviev A. A., Goev A. G., and Kudin D. V. (2026), Coseismic Effect of the 2025 Kamchatka Earthquakes, *Russian Journal of Earth Sciences*, 26, ES2005, EDN: TIGVUI, https://doi.org/10.2205/2026es001115

1. Introduction

Signals that occur simultaneously with the arrival of seismic waves are called coseismic – accompanying seismic waves. Coseismic electromagnetic (CoSEM) signals can arise from the action of elastic waves generated by both earthquakes and industrial explosions [*Anisimov et al.*, 1985]. Initially, in both field observations and experimental and theoretical studies of CoSEM phenomena accompanying strong earthquakes, the main focus was primarily on effects occurring near the source (see, for example, [*Belov et al.*, 1974; *Haartsen and Pride*, 1997]). This type of work was mainly motivated by the search for electromagnetic precursors of strong earthquakes. Below we discuss the effect produced by teleseismic elastic waves generated by distant earthquakes. The resulting CoSEM signals are very similar in shape to seismic records [*Soloviev*, 2023]. In particular, the magnetograms clearly show oscillations corresponding to different seismic phases; the spectra of the CoSEM and seismic disturbances are also consistent with each other [*Kasdi et al.*, 2022; *Soloviev et al.*, 2024]. The similarity between seismic and CoSEM disturbances allows us to consider the latter as a pseudo-seismogram and use it to reconstruct the velocity structure of the upper crust [*Manglik and Gupta*, 2025].

One possible mechanism for the CoSEM effect is geomagnetic inductive disturbance. Forced oscillations of the medium at a velocity $\vec{v}(t)$ in the Earth's magnetic field $\vec{B}$ lead to the generation of an electromotive force $\sim \vec{v}(t) \times \vec{B}$. Due to the finite conductivity of the Earth's crust, this leads to the excitation of an electric current within it, and hence

Research Article

Received: February 2, 2026
Accepted: May 25, 2026
Published: July 1, 2026

the generation of electric and magnetic fields on the Earth's surface. In fluid-saturated rocks, the CoSEM effect may be caused by charge separation [e.g., *Varotsos et al.*, 2013, and references therein]. Under certain conditions, negative ions are absorbed by the solid matrix, while positive ions remain in the fluid, forming an electrical double layer. The presence of excess ions causes the fluid pressure gradient initiated by seismic waves or the accelerated motion of the medium to induce an electric current. This mechanism for excitation of the CoSEM signal is called the electrokinetic effect [e.g., *Surkov et al.*, 2018].

In addition to the mechanisms mentioned above, excitation of CoSEM disturbances can be caused by the mechanical response of the magnetic sensor to seismic waves (the seismographic effect). Specifically, *Eleman* [1966] demonstrates that a mechanical magnetometer with a magnetic needle behaves like an ultra-low-sensitivity seismic recorder, which can be used as an additional seismic station during strong earthquakes. The seismographic effect can also be observed with modern recording equipment [*Masci and Thomas*, 2016], which further highlights the need for a thorough and careful analysis when interpreting disturbances accompanying seismic events [*Soloviev et al.*, 2024]. At the same time, when analyzing magnetotelluric sounding data, the CoSEM effect is interpreted as electrokinetic or electromagnetic [e.g., *Honkura et al.*, 2009]. The nature of CoSEM disturbances is not discussed in this paper.

The kinematic properties of different teleseismic phases differ significantly. Furthermore, the amplitudes of Love and Rayleigh waves are significantly greater than those of both shear and, especially, longitudinal body waves. Therefore, the CoSEM disturbances produced by each phase should generally be studied separately. This means that it is essential to have electromagnetic and, if possible, seismic signal recordings at a significant distance from the earthquake's source, as reliable phase separation occurs at a fairly large epicentral distance. In fact, we are talking about distances of approximately 30 angular degrees (~3,000 km) from the earthquake's source.

The seismoelectric effect of the second kind – the excitation of an electromagnetic field during the propagation of elastic waves in porous, water-saturated rocks – was first described in [*Ivanov*, 1939]. CoSEM disturbances produced by remote earthquakes are often observed in magnetotelluric measurements [e.g., *Honkura et al.*, 2009; *Matsushima et al.*, 2002; *Nagao et al.*, 2000, et al.]. Moreover, the distance from the station to the earthquake source in these studies ranges from 50 to 800 km. Since 2014, a new format has been introduced into the observation practice of magnetic observatories that are part of the global INTERMAGNET network [*Love and Chulliat*, 2013]: precise measurement data with a sampling rate of one second. Among other improvements, the availability of one-second data makes it possible to record CoSEM electromagnetic disturbances [*Soloviev*, 2023]. A significant advantage of using data from observatories is that they operate continuously, unlike most magnetotelluric sounding experiments. The works [*Soloviev*, 2023; *Soloviev et al.*, 2024] explored the CoSEM effect produced by the seismic doublet of strong (magnitude $M_W > 7.0$) Turkish earthquakes of 2023. The first of the cited works showed that the accompanying effect manifests itself at epicentral distances of up to 20 arc degrees (~2,000 km).

In this paper, we limit ourselves to examining issues related to the very possibility of observing CoSEM effects caused by strong distant earthquakes, without discussing their excitation mechanisms. For this purpose, we use elastic waves generated by the "Great Kamchatka Earthquake" (GKamE-2025) – an earthquake on July 29, 2025, with a magnitude of 8.7 and an origin time of 23:24:50 UTC. The GKamE-2025 earthquake is among the top 10 strongest seismic events in the instrumental record. It was accompanied by numerous foreshocks and aftershocks, some exceeding magnitude 7.0. This provides us with a unique opportunity to study the properties of the CoSEM effect produced by distant earthquakes, depending on their magnitude and epicentral distance.

2. Materials and Methods

In [*Soloviev*, 2023], it was noted that even at relatively short distances, the CoSEM signal is generated only by strong earthquakes with magnitudes $M_W > 7.0$. Therefore, in this study, in addition to the main event, we use several of its foreshocks and aftershocks with magnitudes $M_W > 7.0$, which occurred in the same zone as the main shock. In addition, we analyze two more earthquakes, the first of which is an aftershock on August 3, 2025, ($M_W = 6.8$). The second earthquake is an event with $M_W = 7.6$, which occurred on December 8, 2025, at 14:15:10 UTC in the area of the Japanese islands and is not directly related to GKamE (see Table 1 and Figure 1). The source of the main seismic event parameters is the *GCMT* catalog (https://www.globalcmt.org).

Table 1. Catalog of the earthquakes under consideration. M_W is the magnitude.

Latitude, °	Longitude, °	Depth, km	M_W	Date and time, UTC	Focal mechanism
52.51	160.26	18.0	8.7	29 Jul 2025, 23:24:50	
53.19	160.51	19.0	7.8	18 Sep 2025, 18:58:13	
40.997	142.18	45.4	7.6	08 Dec 2025, 14:15:10	
52.90	160.76	20.0	7.4	20 Jul 2025, 06:49:02	
53.10	160.29	39.0	7.4	13 Sep 2025, 02:37:54	
52.92	160.14	29.0	7.0	17 Aug 2024, 19:10:26	
50.58	157.80	35.00	6.8	03 Aug 2025, 05:37:55	

Data from 24 magnetic observatories of the INTERMAGNET standard (see Table 2 and Figure 1) located at distances from 20° to 90° from the GKamE-2025 source are analyzed. The chosen range is determined by two considerations: the left boundary of the interval corresponds to the minimum distance at which complete separation of body and surface waves occurs; the right boundary of the chosen range is close to the maximum distance at which direct volume phases can be observed. This limitation is due to the geometric shadow of the liquid core.

Assuming a linear excitation of the CoSEM disturbances, its spectrum is determined by the frequency content of the original seismic signal, and therefore lies within the range of 0.01 Hz to 0.5 Hz (in periods from 2 s to 100 s). Therefore, when selecting data, observatories with 1-second geomagnetic field recordings are considered. For convenience, instead of magnetic field components, their time derivatives are used; for this, the data are numerically differentiated with respect to time, as described in [*Soloviev*, 2023]. Let us recall that with horizontal homogeneity of the geoelectric properties of the underlying medium, the orientation of the magnetic induction vector $d\mathbf{B}/dt$ corresponds to the direction of the excited telluric field $\mathbf{E}$ and currents in the surface layers of the Earth, i.e., $d\mathbf{B}/dt \sim \mathbf{E}$.

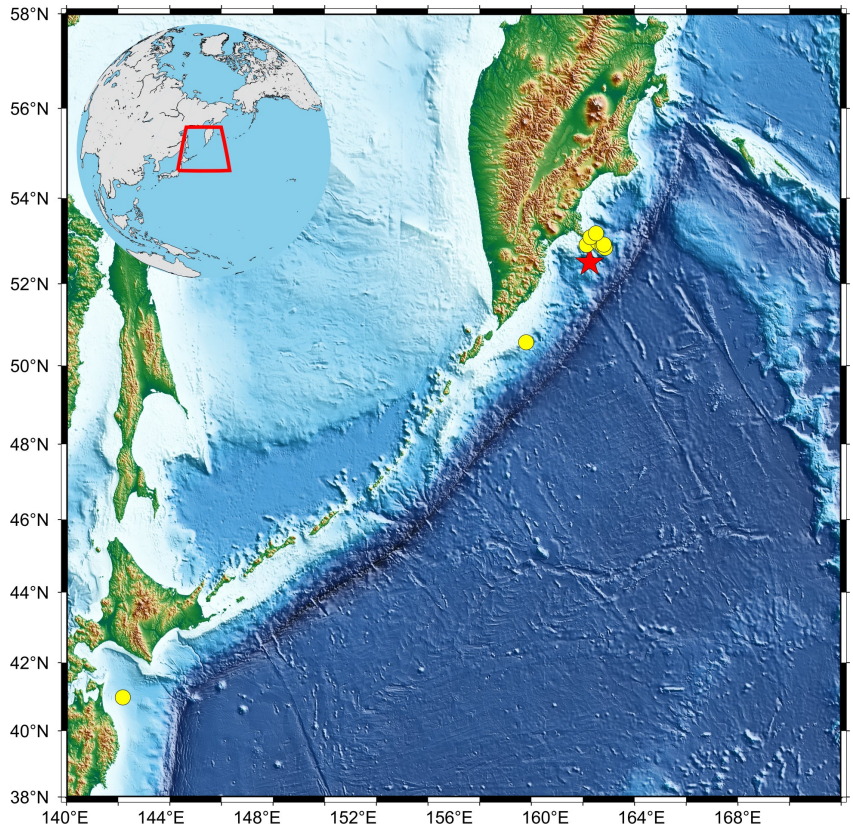

Figure 1. On the left is the distribution of epicenters of the earthquakes under study (yellow circles); on the right is the location of magnetic observatories whose data are used in the study. The main event, GKamE-2025, is marked with a star.

3. Results and Discussion

Coseismic disturbances produced by remote sources are small, so their observation is possible if their amplitude exceeds the noise level. If the noise level is high, the coseismic signal of a relatively weak event may be simply invisible against the background noise, while the amplitude of a strong event may be distorted. To partially suppress the noise component, we use bandpass filtering of the magnetic recordings. Teleseismic phase frequencies range from 2 s to 100 s. Due to Rayleigh scattering and the spectral composition of microseisms, it makes sense to limit the high-frequency part of the signal spectrum to 10 s. As a result, a 4th-order Butterworth bandpass filter with pass periods from 10 s to 80 s is used in the analysis. For convenience, the analysis is carried out in the ray coordinate system Z, R, T, in which the R axis lies in the plane of incidence and is directed toward the epicenter; the T axis is perpendicular to the R axis and the vertical Z axis.

Let us illustrate this with an example of the event of December 8, 2025, recorded at the Mikhnevo geophysical observatory (IAGA code MHV, Moscow Region, Russian Federation). At the time of the seismic wave arrival, two *FGE* vector magnetometers with identical characteristics were simultaneously operating at the observatory [*Pedersen and Merenyi*, 2012]. There were two differences in the instrument setup. First, one was oriented toward the geographic pole, while the other was oriented toward the magnetic pole; this fact becomes irrelevant after converting to a ray coordinate system. Second, the three-axis sensor of one magnetometer was mounted on a suspension, while the other sensor was firmly fixed to the instrument base. Sections of the magnetograms recorded by these two instruments during the arrival of the seismic signal (Figure 2, top panel) from the above-mentioned event are shown in the middle and bottom panels of Figure 2, respectively. The figure shows that the coseismic effect associated with surface waves is clearly visible in the $d\mathbf{B}/dt$ records from the suspended instrument; CoSEM disturbances caused by body shear

Table 2. INTERMAGNET magnetic observatories whose data were used in this study. The columns list the observatory codes, their latitudes and longitudes, azimuths, and epicentral distances to GKamE-2025. The observatories are sorted by epicentral distance and grouped by this parameter; the groups are highlighted in color.

Code	Latitude, °	Longitude, °	Azimuth, °	Δ, °
SHU	55.35	199.54	67.2	23.1
BRW	71.32	203.38	29.3	26.7
CMO	64.87	212.14	44.3	28.7
GUA	13.59	144.87	203.3	40.7
CBB	69.12	254.97	31.0	43.9
HON	21.32	202.0	118.0	44.7
AAA	43.25	76.92	295.8	53.7
FRN	37.09	240.28	71.9	55.9
KLI	60.85	39.51	330.1	57.5
SPG	60.54	29.71	334.4	60.6
MHV	54.95	37.76	326.8	62.8
TUC	32.17	249.27	69.8	64.6
KDU	−12.69	132.47	209.1	69.2
API	−13.82	188.22	151.1	70.3
WNG	53.73	9.05	342.4	71.4
NGK	52.07	12.68	339.7	72.3
CTA	−20.09	146.26	193.7	73.3
FRD	38.21	282.63	43.1	76.7
ASP	−23.76	133.88	204.5	79.4
PEG	38.10	23.9	326.7	82.1
CKI	−12.19	96.83	241.5	84.2
LRM	−22.22	114.1	222.2	84.6
EBR	40.96	0.33	344.9	85.3
SPT	39.55	355.65	348.1	87.3

waves are discernible, but less clearly visible. For longitudinal waves, the signal amplitude apparently does not exceed the noise level.

The magnitude of electromagnetic "noise" (natural variations in the electromagnetic field and measurement interference) can be estimated from the amplitude of the variations recorded before the *P*-wave arrival. Figure 2 shows that when the sensor is mounted using a suspension, the noise component is significantly lower than when it is fixed directly on a pillar. This is particularly noticeable in the *Z* component, where the ratio of the amplitudes of the noise terms is ~3.

After high-pass filtering with a 4th-order Butterworth bandpass filter with pass periods from 30 to 80 seconds, the differences between the magnetograms from both instruments virtually disappear; at the same time, the coseismic signal also disappears (Figure 3). More precisely, the amplitude of the coseismic disturbances in this frequency range does not exceed the noise amplitude. This allows us to conclude that the high-frequency portion of the spectrum plays a significant role in the observation of the CoSEM effect. The described experiment requires further study; the interpretation provided is purely preliminary.

The energy released during an earthquake is distributed unevenly between seismic phases, with longitudinal waves having the minimum amplitude and surface waves having the maximum. The *P* and *S* volume phases, in addition to polarization and amplitude, differ in the shape of the function at the source and the geometric parameters of the trajectory. The most significant difference between body and surface (Rayleigh and Love)

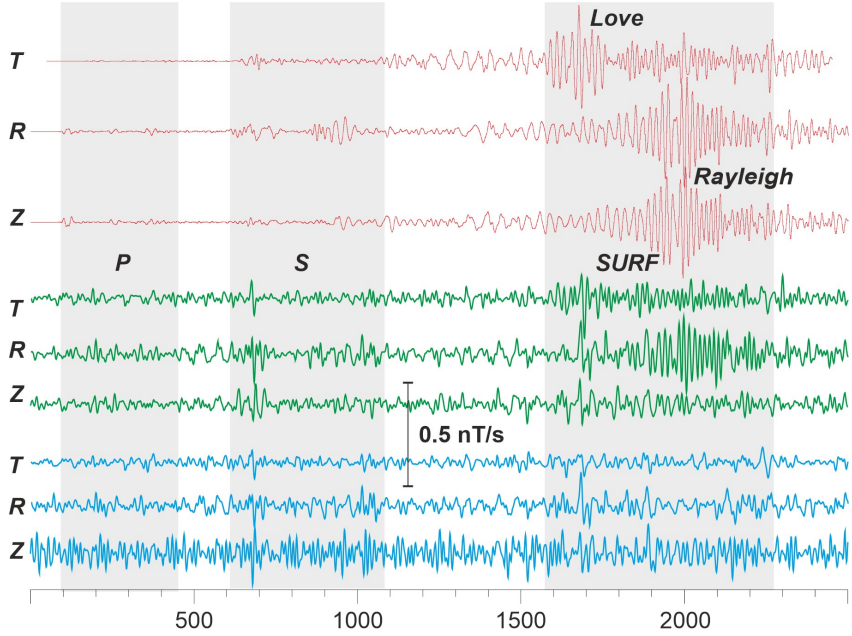

Figure 2. Seismograms (upper panel, red curves) and d**B**/dt time series (middle and lower panels) of the event on December 8, 2025 recorded at the Mikhnevo geophysical observatory (Moscow Region, Russian Federation). Magnetic data were recorded by two three-component variometers, one of which is mounted on a suspension (green traces), and the second is fixed directly on a pillar (lower traces, blue). The gray rectangles mark the time domain of seismic phase oscillations – body longitudinal (P), shear (S), and surface (SURF). The vertical scale of magnetic measurements is indicated in the center of the figure; the abscissa axis represents time in seconds, starting 100 s before the arrival of the P-wave according to the IASP91 standard model [*Kennett and Engdahl*, 1991].

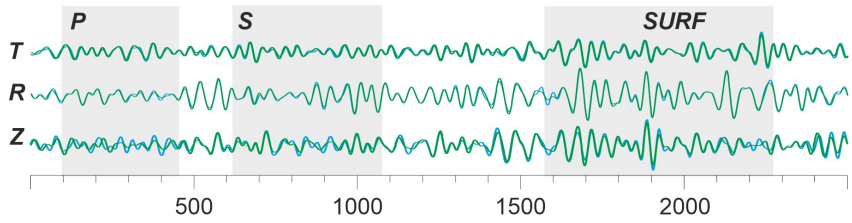

Figure 3. Recordings from both vector magnetometers (with superimposed components) after high-pass filtering. The notations are the same as in the previous figure.

waves relates to their propagation paths: body waves penetrate the Earth's interior to the mantle depths, while surface waves propagate along the surface. Therefore, the detection of CoSEM disturbances is conducted separately for these three wave types.

As shown in [*Soloviev et al.*, 2024], observation of CoSEM disturbances depends heavily on the earthquake's magnitude and epicentral distance. Magnitude characterizes the energy released by the earthquake, and therefore the initial wave amplitude, while epicentral distance determines the reduction in this amplitude due to geometric spreading, scattering, and attenuation. Clearly, given the assumed linearity of the CoSEM effect, these two factors play a crucial role in its observation.

In this study, the influence of seismic radiation directionality on the recording of the CoSEM effect is minimized. This is indicated by two key factors: first, the sufficiently dense azimuthal coverage of observation points relative to the source area (see Figure 1); second, earthquakes with different focal mechanisms are included in the analysis (see Table 1). Since the focal mechanism determines the directivity graph of the body wave radiation (including the polarity and amplitude of P- and S-waves), the processing of events with different types of focal mechanisms also neutralizes the influence of a specific type of source on the manifestation of the effect under study.

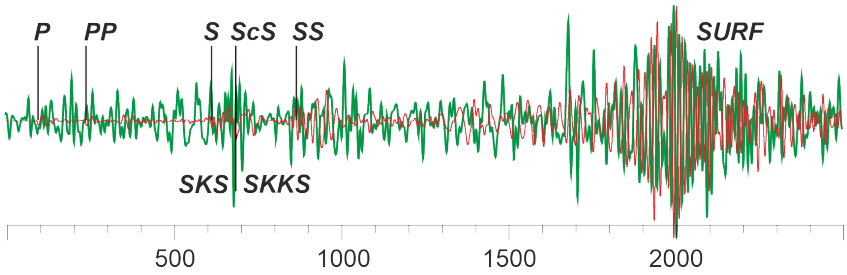

Figure 4. *R* components of the seismic (red curve) and magnetic (green curve) signals of the GKamE-2025 event, recorded at the Mikhnevo observatory (epicentral distance 63°). In addition to the main *P* and *S* body waves, the seismogram also contains phases formed by reflection from the ground surface (*PP*, *SS*) and interaction with the core-mantle boundary (*ScS*, *SKS*, *SKKS*). CoSEM disturbances produced by longitudinal waves, if present, have an amplitude that does not exceed the electromagnetic background; the CoSEM signal of shear and surface waves is clearly recorded.

To minimize the influence of random factors and spatial heterogeneity in the distribution of recording equipment, the selected observatories are grouped by epicentral distance. We use six ranges (in arc degrees): 20–30, 40–45, 50–60, 60–70, 70–80, and 80–90 (see Table 1). For each seismic event, magnetograms at all observatories in the group are examined for the presence of a CoSEM signal. A result for a group is considered positive if a disturbance is recorded at least at one observatory. Signal presence is determined separately for each phase. Obviously, the shape of the CoSEM disturbances in magnetogram components may not match the shape of the corresponding seismic records, so when detecting them, we focus on the increase in magnetic field amplitude at the arrival times of the corresponding waves. At large epicentral distances (starting from approximately 50°), the arrival time of the main *S*-wave is close to the arrival times of one or more phases formed at internal seismic boundaries (see Figure 4). Since the objective of this study is to register the presence or absence of CoSEM disturbances as such, a separate analysis of the CoSEM effect from different phases is not conducted.

Table 3. Distribution of mechanisms of aftershocks of the Kamchatka earthquake for the period July 29 – December 31, 2025 according to the types of movement in the source based on classification according to the plunge angles of the main axes

Mw	20–30			40–45			50–60			60–70			70–80			80–90		
	P	*S*	*SURF*	*P*	*S*	*SURF*	*P*	*S*	*SURF*	*P*	*S*	*SURF*	*P*	*S*	*SURF*	*P*	*S*	*SURF*
8.7																		
7.8																		
7.6																		
7.4																		
7.0																		
6.8																		

The results of a comparison of geomagnetic and seismic measurements are presented in Table 3. If the magnitude of an event does not exceed 7.0, the resulting CoSEM effect is not observed even at relatively close observatories. On the other hand, waves generated by earthquakes with even greater magnitudes (in our case, with $M_W \geq 7.4$) are capable of

producing CoSEM disturbances at epicentral distances of up to 90°, which is the limit for direct body waves.

4. Conclusion

The conducted studies show that the CoSEM signal of teleseismic waves recorded by the INTERMAGNET magnetic observatories is primarily evident at periods between 1 and 30 seconds. The presence of noise in this period range can obscure or significantly suppress the coseismic component. Therefore, a prerequisite for its observation is the availability of high-quality 1-second geomagnetic field recordings at the observation sites. The wide spatial distribution of observatories and continuous geomagnetic field measurements make it possible to study the properties of the CoSEM disturbances caused by earthquakes at arbitrary epicentral distances.

The source of the CoSEM disturbances under study are the seismic waves emitted by GKamE-2025, as well as its foreshocks and aftershocks. Rather large number of events with magnitudes $M > 7$, localized in a relatively small area, increase the statistical significance of the analysis. It turns out that the CoSEM effect generated by body waves manifests itself at extreme epicentral distances if the source of these waves is the strong earthquakes with a magnitude of $M > 7.0$. However, we note that for events with a magnitude of $M < 7.0$, the generated waves do not produce a noticeable CoSEM effect even at relatively close epicentral distances.

Acknowledgments. The authors are sincerely grateful to E. Yu. Sokolova (All-Russian Research Geological Oil Institute, Schmidt Institute of Physics of the Earth of the Russian Academy of Sciences) for her attention to this work, discussion of the results, and critical comments. The authors are also grateful to two anonymous reviewers for their detailed study of the manuscript and valuable comments. This work utilizes data and services from the Analytical Geomagnetic Data Center of the Geophysical Center of the Russian Academy of Sciences (https://ckp-rf.ru/catalog/ckp/435997). The results presented in this paper also rely on data collected at magnetic observatories. We thank the national institutes that support them, INTERMAGNET for promoting high standards of magnetic observatory practice (http://www.intermagnet.org), and the Analytical Geomagnetic Data Center (https://mag.gcras.ru) for free distribution of data online. The work was carried out within the framework of state assignments of the Geophysical Center of the Russian Academy of Sciences and the Schmidt Institute of Physics of the Earth of the Russian Academy of Sciences, approved by the Ministry of Education and Science of the Russian Federation.

References

Anisimov S. V., Gokhberg M. B., Ivanov E. A., et al. Short-period oscillations of the geomagnetic field induced by industrial explosion // Doklady Akademii Nauk SSSR. — 1985. — Vol. 281, no. 3. — P. 556–559. — (In Russian).

Belov S. V., Migunov N. I. and Sobolev G. A. Magnetic effect of strong earthquakes in the Kamchatka region // Geomagnetism and Aeronomy. — 1974. — Vol. 14, no. 3. — P. 380–382.

Eleman F. The Response of Magnetic Instruments to Earthquake Waves // Journal of Geomagnetism and Geoelectricity. — 1966. — Vol. 18, no. 1. — P. 43–72. — https://doi.org/10.5636/jgg.18.43

Haartsen M. W. and Pride S. R. Electroseismic waves from point sources in layered media // Journal of Geophysical Research: Solid Earth. — 1997. — Vol. 102, B11. — P. 24745–24769. — https://doi.org/10.1029/97jb02936

Honkura Y., Ogawa Y., Matsushima M., et al. A model for observed circular polarized electric fields coincident with the passage of large seismic waves // Journal of Geophysical Research: Solid Earth. — 2009. — Vol. 114, B10. — https://doi.org/10.1029/2008jb006117

Ivanov A. G. Effect of electrification of Earth layers during the passage of elastic waves through them // Doklady Akademii Nauk SSSR. — 1939. — Vol. 24, no. 1. — P. 41–43. — (In Russian).

Kasdi A. S., Bouzid A. and Hamoudi M. Electromagnetic Signal Associated with Seismic Waves: Case Study in the North Central Algeria Area // Pure and Applied Geophysics. — 2022. — Vol. 179, no. 5. — P. 1965–1979. — https://doi.org/10.1007/s00024-022-03020-0

Kennett B. L. and Engdahl E. R. Traveltimes for global earthquake location and phase identification // Geophysical Journal International. — 1991. — Vol. 105, no. 2. — P. 429–465. — https://doi.org/10.1111/j.1365-246x.1991.tb06724.x

Love J. J. and Chulliat A. An International Network of Magnetic Observatories // Eos, Transactions American Geophysical Union. — 2013. — Vol. 94, no. 42. — P. 373–374. — https://doi.org/10.1002/2013eo420001

Manglik A. and Gupta S. Coseismic Electromagnetic Signals as Pseudo-Seismograms for Mapping of Upper Crustal Seismic Velocity Structure: An Example from the Ganga Basin Using Magnetotelluric Time Series of the 3 November 2023 Western Nepal Earthquake // Journal Of The Geological Society Of India. — 2025. — Vol. 101, no. 6. — P. 809–814. — https://doi.org/10.17491/jgsi/2025/174165

Masci F. and Thomas J. N. Evidence of underground electric current generation during the 2009 L'Aquila earthquake: Real or instrumental? // Geophysical Research Letters. — 2016. — Vol. 43, no. 12. — P. 6153–6161. — https://doi.org/10.1002/2016gl069759

Matsushima M., Honkura Y., Oshiman N., et al. Seismoelectromagnetic Effect Associated with the Izmit Earthquake and Its Aftershocks // Bulletin of the Seismological Society of America. — 2002. — Vol. 92, no. 1. — P. 350–360. — https://doi.org/10.1785/0120000807

Nagao T., Orihara Y., Yamaguchi T., et al. Co-seismic geoelectric potential changes observed in Japan // Geophysical Research Letters. — 2000. — Vol. 27, no. 10. — P. 1535–1538. — https://doi.org/10.1029/1999gl005440

Pedersen L. W. and Merenyi L. The FGE Magnetometer and the Intermagnet 1 Second Standard // XVIth IAGA Workshop on Geomagnetic Observatory Instruments Data Acquisition and Processing. — Hyderabad, India : IAGA, 2012.

Soloviev A. A. Geomagnetic Effect of the Earthquakes with Mw = 7.5-7.8 in Turkey on February 6, 2023 // Doklady Earth Sciences. — 2023. — Vol. 511, no. 1. — P. 578–584. — https://doi.org/10.1134/s1028334x23600731

Soloviev A. A., Aleshin I. M., Anisimov S. V., et al. The Fine Structure of Coseismic Electromagnetic Response Based on Geomagnetic and Seismological Observations // Izvestiya, Physics of the Solid Earth. — 2024. — Vol. 60, no. 5. — P. 891–902. — https://doi.org/10.1134/s1069351324700812

Surkov V. V., Pilipenko V. A. and Sinha A. K. Possible mechanisms of co-seismic electromagnetic effect // Acta Geodaetica et Geophysica. — 2018. — Vol. 53, no. 1. — P. 157–170. — https://doi.org/10.1007/s40328-018-0211-6

Varotsos P. A., Sarlis N. V., Skordas E. S., et al. Seismic Electric Signals: An additional fact showing their physical interconnection with seismicity // Tectonophysics. — 2013. — Vol. 589. — P. 116–125. — https://doi.org/10.1016/j.tecto.2012.12.020